PERGAMON

International Journal of Heat and Mass Transfer 45 (2002) 3609–3619

International Journal of HEAT and MASS TRANSFER

www.elsevier.com/locate/ijhmt

Heat transfer in pulse-stabilized fluidization – Part 1: overall cylinder and average local analyses

Deborah V. Pence [a,*], Donald E. Beasley [b]

[a] Department of Mechanical Engineering, Oregon State University, 204 Rogers Hall, Corvallis, OR 97331, USA
[b] Department of Mechanical Engineering, Clemson University, P.O. Box 340921, Clemson, SC 29634, USA

Received 19 November 2000; received in revised form 31 January 2002

Abstract

The present study examines the effect of an opposing oscillatory flow on heat transfer from an immersed horizontal cylinder in a bubbling gas-fluidized bed. This opposing oscillatory flow creates a state of fluidization termed pulse-stabilized fluidization. Heat transfer rates were measured for a monodisperse distribution of particles for fluidization ratios ranging from 1.1 to 2.7. Overall heat transfer measurements from a submerged horizontal cylinder show that the heat transfer characteristics are significantly altered by an opposing oscillatory flow. A modified form of the Strouhal number effectively characterizes the particle Nusselt number. Time-averaged local heat flux measurements showed that the local heat transfer distribution was altered by the hydrodynamics induced by the opposing oscillatory flow.

1. Introduction

Typical bubbling fluidized beds are adversely affected by the behavior of coal fines, which cause high levels of elutriation and increased emissions due to combustion in the freeboard region. The pulsed atmospheric fluidized bed combustor (PAFBC), as shown in Fig. 1, provides significant advantages for the combustion of coal fines by employing a pulsed combustor, while maintaining the reduced emissions and high heat transfer rates of a bubbling fluidized bed. In the hybrid PAFBC, coal fines are burned in a pulsed combustor that faces vertically downward in the bubbling fluidized bed. The pulsed combustor introduces a secondary flow of high temperature combustion gases into the bed. This secondary flow has an exit velocity that consists of a sinusoidally oscillating component superimposed on a steady mean flow. The technology has been successfully demonstrated on the campus of Clemson University under the auspices of the DOE Clean Coal Program and the South Carolina Institute for Energy Studies (SCIES). Fluidization was more stable and heat transfer rates were significantly enhanced in the PAFBC demonstration over those typical of a bubbling fluidized bed combustor. Further description of the PAFBC concept and operation is provided in [1].

For the present study, an experimental model of the PAFBC was constructed which allowed the effect of an oscillating secondary flow on fluidization characteristics and heat transfer to be determined. The global hydrodynamics in the bubbling bed are significantly altered by the presence of the secondary flow [2]. For example, traditional fluidized beds have overall circulation patterns that are generally upwards in the center and downwards at the walls. The introduction of the secondary flow in the present facility created a markedly different overall circulation pattern, with solids generally migrating upwards near the walls, and downward along the pulsed flow simulator tailpipe. For most operating conditions, the introduction of the oscillating component of the secondary flow also created an obvious periodic behavior of the bubble generation and movement of the free surface of the bed. These hydrodynamics, termed "pulse-stabilized fluidization", are documented in [3].

* Corresponding author. Tel.: +1-541-737-7018; fax: +1-541-737-2600.
E-mail address: pence@engr.orst.edu (D.V. Pence).

0017-9310/02/$ - see front matter
PII: S0017-9310(02)00067-4

Nomenclature

A_{eff}	effective area of heat flux probe (m^2)
A_s	surface area of horizontal copper cylinder (m^2)
d_p	mean particle diameter (m)
d_t	inside diameter of pulsed flow simulator tailpipe (m)
$E(t)$	time varying bridge circuit voltage (V)
E_b	time-averaged bridge circuit voltage for constant probe temperature (V)
E_c	potential supplied to cartridge heater (V)
f	forcing frequency of piston (Hz)
f_n	natural frequency of pulsed flow simulator (Hz) ($f_n = 26$ Hz)
h	overall cylinder heat transfer coefficient (W/m^2 K)
h_{eq}	overall heat transfer coefficient with an equivalent flow, Q_{eq}, through the plenum (W/m^2 K)
$h_{eq,\theta}$	time-averaged local heat transfer coefficient measured at angular position θ with an equivalent flow through the plenum (W/m^2 K)
h_f	overall cylinder heat transfer coefficient acquired with a secondary flow forced at f Hz (W/m^2 K)
$h_{f,\theta}$	time-averaged local heat transfer coefficient measured at θ with a secondary flow forced at f Hz (W/m^2 K)
$h_{p,\theta}$	time-averaged local heat transfer coefficient measured at θ with a primary flow only (W/m^2 K)
h_θ	time-averaged local heat transfer coefficient (W/m^2 K)
h_0	overall cylinder heat transfer coefficient acquired with a steady secondary flow (W/m^2 K)
$h_{0,\theta}$	time-averaged local heat transfer coefficient measured at θ with a steady secondary flow (W/m^2 K)
I_c	current supplied to cartridge heater (A)
k_f	thermal conductivity of air at 300 K (W/m K)
Nu_p	Nusselt number based on particle diameter ($Nu_p = hd_p/k_f$)
Q_{eq}	equivalent flow rate: total flow rate, Q_t, is introduced through plenum (m^3/s)
Q_{mf}	flow rate corresponding to minimum fluidization (m^3/s)
Q_p	primary flow rate, plenum (m^3/s)
Q_s	secondary flow rate, pulsed flow simulator (m^3/s)
Q_t	total flow rate: sum of primary and secondary flow rate (m^3/s)
r	driving link radius for pulsed flow simulator (m)
r_1	resistance in leg one of bridge circuit (Ω)
r_2	resistance in leg two of bridge circuit (Ω)
r_{decade}	decade resistance bridge circuit (Ω)
R_b	bridge circuit resistance (10 Ω)
R_c	cable resistance (Ω)
R_p	probe resistance (Ω)
St	Strouhal number ($St = d_t f/U_s$)
St'	modified Strouhal number ($St' = St(f/f_n)^{-0.8}$)
T_b	average temperature of fluidized bed media (°C)
T_p	probe temperature (°C)
T_s	surface temperature of horizontal copper cylinder (°C)
U_s	mean velocity at exit of pulsed flow simulator tailpipe (m/s)
V_k	kinematic velocity amplitude at exit of pulsed flow simulator tailpipe (m/s)
V_r	resonant velocity amplitude at exit of pulsed flow simulator tailpipe (m/s)

Greek symbol

θ	angular position around horizontal cylinder: measured from stagnation point (°)

Bubbling fluidized beds may be characterized as self-excited, nonlinear systems. Under typical operating conditions pressure, void fraction and heat transfer in bubbling fluidized beds have been shown to behave in a manner consistent with deterministic chaos [4–6]. The extreme sensitivity to initial conditions associated with chaos suggests the possibility of control or optimization of chaotic states with carefully chosen perturbation of the operating conditions. Recently, the present authors have successfully demonstrated chaos suppression of the hydrodynamics using pulse-stabilized fluidization [3]. In light of the strong coupling that exists between the hydrodynamics and heat transfer in bubbling fluidized beds, the potential for using a secondary flow as a perturbation parameter for active or passive chaos control of a fluidized bed seems plausible. However, to make such active or passive control possible, the influence of pulse-stabilization on heat transfer must first be investigated.

In the present work, the influence of pulse-stabilized fluidization on heat transfer is investigated in two parts. In Part 1 of this paper, the effects of an opposing os-

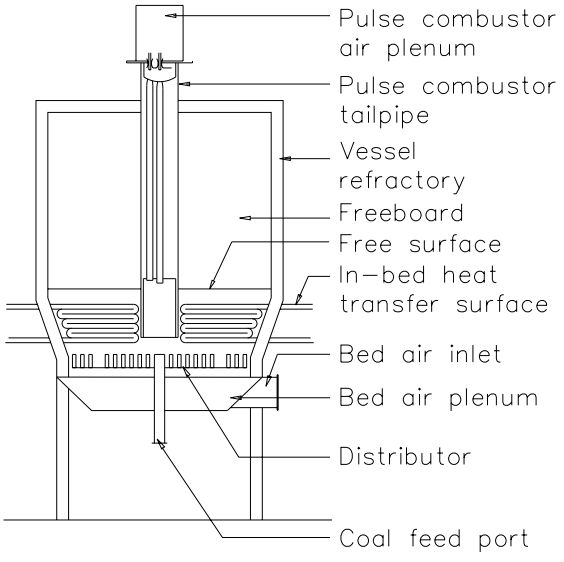

Fig. 1. Pulsed atmospheric fluidized bed combustor (PAFBC).

cillatory flow on overall and local time-averaged heat transfer are examined. Part 2 examines the local, instantaneous measurements of heat flux as a function of angular position around the circumference of the heated cylinder. Results are presented that document the effects of significant changes in the hydrodynamics of fluidization resulting from pulse-stabilization on heat transfer.

2. Background

Overall heat transfer from a single horizontal cylinder submerged in a bubbling gas-fluidized bed has been extensively investigated and numerous correlations developed for predicting the overall and maximum overall heat transfer coefficients achievable for these operating conditions. Ainshtein and Gel'perin [7] and Grewal and Saxena [8] summarize a number of these.

Kobayashi et al. [9] experimentally investigated the effects of pulsing the plenum stream of a gas-fluidized bed on the rates of heat transfer. On/off pulsing of the flow stream resulted in an attenuation of the bubbling phenomenon, shorter particle residence times, and a lower bubble fraction compared with the same flow rate in an unpulsed fluidizing stream. Increases in heat transfer were attributed to active particle mixing below minimum fluidization [10].

Using a hot film anemometer, Nowak et al. [11] measured the relative enhancements in time-averaged heat transfer coefficients in a bed of monodispersed fine, cohesive particles subjected to an opposing acoustic field, and compared these values to those measured in a bed with no acoustic field. In both cases, an extremely low primary flow was employed. When no acoustic flow was present, the bed remained fixed due to particle agglomeration. Increases in heat transfer ranged from 100% to 200% for a range of low primary flow rates when the bed was acoustically forced at 20 Hz. This frequency corresponded to the resonant frequency of the system consisting of the pipe between the loudspeaker and the free surface of particles. Moussa and Fowle [12] also examined the effects on combustion of pulsations in the fluidizing flow.

Yates et al. [13], Shen et al. [14], and Ding and Gidaspow [15] each employed a secondary gas stream in opposition to the plenum air stream to enhance particle mixing. In each of their experimental facilities, the jet exit was submerged in the gas-fluidized bed, and the effects of the jet penetration depth and variations in void fraction surrounding the secondary flow inlet tube were analyzed. No investigations of the heat transfer mechanisms were performed.

Botterill et al. [16] and George and Welty [17] measured time-averaged local heat transfer coefficients at various angular positions around a single horizontal cylinder in a high temperature bed. Chandran et al. [18] and Kurosaki et al. [19,20] measured heat transfer from a heated horizontal cylinder to a cold bed of fluidized particles. Each investigator reported that, as the fluidization ratio was increased, the heat transfer coefficients remained relatively symmetric about the stagnation point, the angular variations became less pronounced, and the maximum heat transfer coefficient migrated from the sides to the upper portion of the cylinder. Local heat transfer coefficients from a cylinder located in a single row of tubes submerged in hollow polystyrene spheres were measured by Kumada et al. [21]; the bed was fluidized to a flow rate twice that required for minimum fluidization. An increase in heat transfer at the upper portion of the cylinder was observed with increasing flow rate, with the maximum heat transfer coefficient identified at 180° from the stagnation point.

3. Experimental facility

The experimental facility shown in Fig. 2 was designed and instrumented to independently examine the effects of the secondary flow rate and the secondary flow oscillations on pressure and heat transfer in pulse-stabilized fluidization. The facility included provisions for measuring (1) overall heat transfer, and (2) local, instantaneous heat transfer, from which (3) local, time-averaged heat transfer could be determined. Part 1 of this paper focuses on overall and local, time-averaged heat transfer.

Uniform fluidization was achieved using a porous polyethylene distributor plate with a 40 μm mean pore

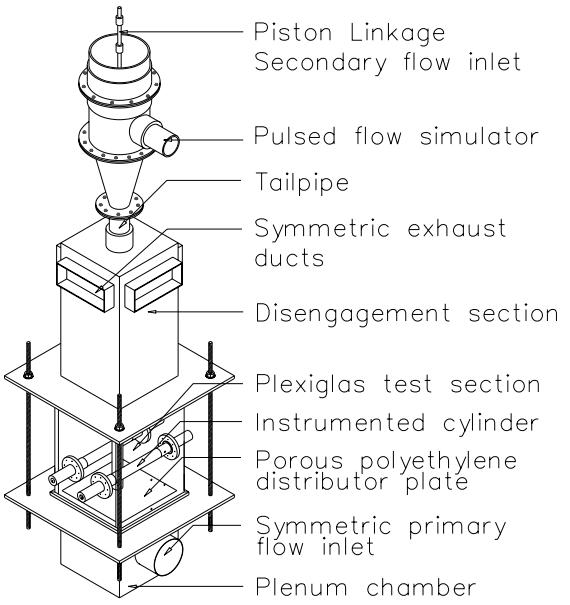

Fig. 2. Experimental facility.

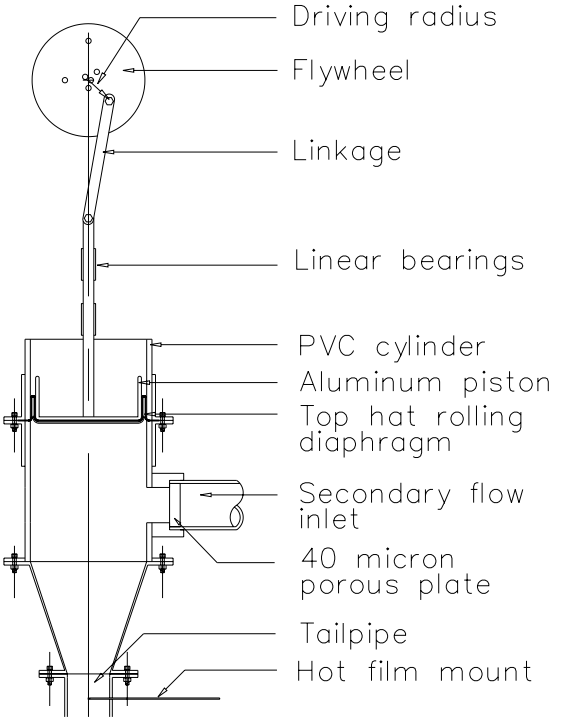

Fig. 3. Pulsed flow simulator.

diameter. The pressure drop across the plate ranged from 100% to greater than 200% of that across the 0.305 m slumped depth of particles constituting the bed. The test section had a cross-sectional flow area of 0.305 m × 0.305 m(1 ft × 1 ft), and a height of 0.53 m. The fluidized particulate was spherical glass beads having a narrow size distribution (monodisperse) with a weight mean diameter of 345 μm and a density of 2.5 g/cm^3. Air was used as the fluidizing medium for both the primary and secondary streams. Airflow rates were measured using orifices that were calibrated using a laminar flow element as a standard. Typical uncertainties in the primary and secondary flow rates range from 2% to 3%.

The oscillating secondary flow field was created by a pulsed flow simulator, shown in Fig. 3, that consisted of a steady flow inlet, a reciprocating piston sealed with a rolling diaphragm, and a tailpipe assembly. The tailpipe, a 3.8 cm PVC tube, extended vertically downward into the test section. The clearance between the end of this tube and the distributor, in proportion with the pilot scale PAFBC, was approximately 1.25 cm. The frequency of the oscillation was controlled through a speed control on the driving motor. The amplitude was controlled by the driving radius, which was fixed at 14.15 mm for this study, unless otherwise stated.

Under appropriate conditions, the facility created a fully reversing (i.e., sinusoidal) secondary flow, typical of pulsed combustors. The pulsed flow simulator tailpipe assembly operated in frequency and amplitude ranges where significant resonance occurred, as determined from measurements of the centerline velocity at the tailpipe exit in absence of the fluidized bed. A model was developed from measured amplitudes at the tailpipe exit that allowed prediction of the resonant amplitude; the model was based on a Helmholtz resonator and an effective tailpipe diameter. The model predictions agreed to within 5% of measured amplitudes. Table 1 shows the kinematic velocity amplitude based on the piston displacement and continuity, and the velocity amplitude computed from the resonance model for a given driving link radius and driving frequency of the piston. Clearly, some degree of uncertainty exists concerning the flow field in the pulsed flow simulator when the fluidized bed was operating. The approach taken in the present study was to report the imposed frequency and amplitude at the piston, and to infer the velocity amplitude at the pulsed flow simulator exit from the resonance model.

To simulate heat transfer surfaces, two horizontal cylinders, each 3.8 cm in diameter, were positioned 15.25 cm above the distributor plate. One cylinder was fabricated from solid copper and instrumented with a TSI model 1471 platinum film heat flux probe. A 1200 W cartridge heater was used to heat the copper cylinder to a temperature approximately 35 °C above the average bed temperature. Delrin was used to insulate the ends of the cylinder, which reduced conduction losses to less than 3%.

Table 1
Resonance analysis for pulsed flow simulator

Flywheel radius r (mm)	Forcing frequency f (Hz)	Kinematic velocity amplitude V_k (m/s)	Resonant velocity amplitude V_r (m/s)
4.25	15	9.6	14.0
	30	19.1	69.6
8.50	10	12.8	14.9
	15	19.1	28.1
14.15	5	10.6	11.0
	10	21.3	24.8
	15	31.9	46.8
	20	42.5	98.1
21.2	5	15.9	16.5
	10	31.9	37.1
	15	47.8	70.2

The overall heat transfer coefficient was calculated from

$$h = \frac{E_c I_c}{A_s(T_s - T_b)}, \quad (1)$$

where E_c and I_c represent the voltage and current, respectively, supplied to the cartridge heater, and A_s represents the surface area of the copper cylinder. The bed temperature, T_b, was averaged from four type-J thermocouples. The surface temperature of the cylinder, T_s, was determined from a temperature measurement 9.5 mm below the surface of the cylinder. The true surface temperature was approximated using a one-dimensional radial conduction model, assuming that the cartridge heater axis was concentric with that of the copper cylinder. The difference between the measured internal temperature and predicted surface temperature was typically 0.4 °C.

Local heat flux measurements were accomplished using the platinum film probe that was flush mounted at the surface of the cylinder. The probe, shown in Fig. 4, was composed of a platinum strip approximately 1.2 mm × 0.3 mm deposited on a Pyrex substrate disk 1.5 mm in diameter and 0.7 mm thick. A 9 μm aluminum oxide coating protected the platinum from erosion in the harsh environment of the fluidized bed. The heat flux probe was maintained at a constant temperature using an anemometer bridge circuit shown schematically in Fig. 4. To ensure bridge stability, the temperature of the probe was maintained at 0.75 °C above the surface temperature of the copper cylinder.

The cylinder and probe were heated and allowed to reach steady-state, for a fixed operating condition. Variations in bridge voltage with time, required to maintain a constant probe temperature, were recorded for 33 s at a sampling frequency of 500 Hz. Spectral

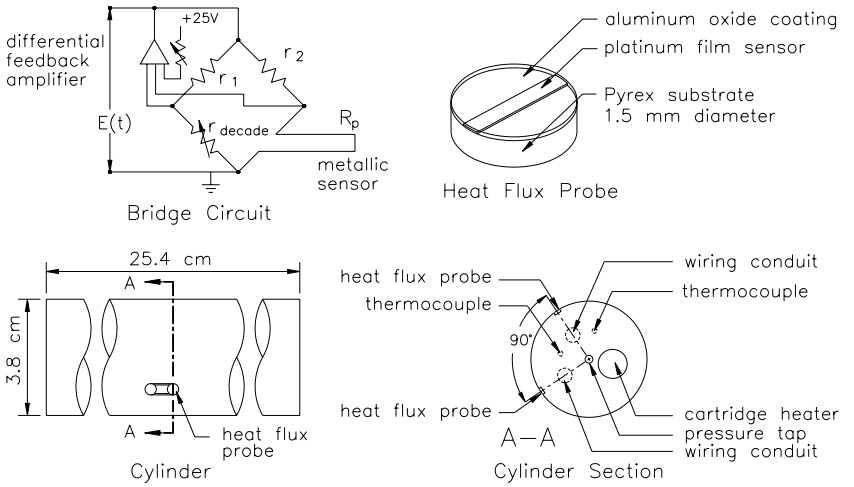

Fig. 4. Instrumented horizontal cylinder, heat flux probe and bridge circuitry.

analysis of preliminary signals indicated that these sampling conditions were appropriate. The heat flux probe had an experimentally measured response time between 2 and 3 ms, allowing measurement of frequency content more than twice the maximum expected frequency of 100 Hz with amplitude errors less than 10%. The data acquisition system consisted of a Keithley/Metrabyte 12-bit A/D board; interfacing with the board was accomplished using Labtech Notebook software.

Local heat transfer rates were determined by time averaging instantaneous measurements. Conversion of the bridge voltage variations to instantaneous heat transfer coefficients was accomplished through an in situ calibration, using the effective area of the heat flux probe as the calibration constant. The effective area, A_{eff}, was determined by forcing the area-weighted average of the time-averaged local heat transfer coefficients, h_θ, to be equal to the overall heat transfer coefficient, h. The following two equations, in conjunction with Eq. (1), illustrate the procedure

$$h = \frac{\sum_{\theta=0}^{315} h_\theta}{8}, \tag{2}$$

where h_θ was measured at 45° increments, and is defined by

$$h_\theta = \frac{E_b^2 R_p}{\left(R_p + R_b + R_c\right)^2 A_{\text{eff}} (T_p - T_b)}. \tag{3}$$

Further descriptions of the characteristics of film probes employed for heat flux measurement and the in situ calibration process are found in [22–24]. Uncertainty in overall and time-averaged local heat transfer coefficients is on the order of 4% and 6%, respectively.

4. Results

Results are presented that quantify the effects of a steady secondary flow and a secondary flow with an oscillating component on the overall and local, time-averaged heat transfer rates. Because there are two flow streams, primary and secondary, associated with pulse-stabilized fluidization the distribution of flow between the two streams is an important parameter in the fluidization conditions. In the present context, distribution of the flow represents a concept of proportioning a total flow rate between the primary and secondary streams. Also, the *primary* flow refers to air that entered the facility through the plenum chamber and the distributor plate. The *secondary* flow entered the facility through the tailpipe of the pulsed flow simulator, and was either steady or had a superimposed oscillatory waveform.

The effects of changes in the total flow rate through the bed, the distribution of the flow between the two opposing streams, and the pulse frequency on heat transfer coefficients are identified through carefully derived normalization methods. The following comparisons for heat transfer coefficients were employed:

- Because of the self-actuating nature of the pulsed combustor in the PAFBC, no additional pumping power is associated with the secondary flow. Therefore, a comparison of the heat transfer before and after a secondary flow is imposed, i.e., a comparison in which the primary flow was the same between the two tests, is meaningful.
- To assess the effect of the flow distribution between the two streams, heat transfer with both primary and secondary flow is compared with the heat transfer measured with a plenum flow only, at a rate equal to the combined flow rate of the primary and secondary streams. This flow through the plenum is termed the *equivalent* flow condition and denoted by a subscript of 'eq'.
- As noted in Table 1, increases in forcing frequency for a fixed driving-link radius results in an increase in the amplitude of the exit velocity, in the absence of particles in the bed. The effect of pulsing characteristics, which include pulse frequency and pulse amplitude, are examined by comparing the heat transfer for an oscillating secondary flow condition with the heat transfer for a steady secondary flow condition.

Superficial flow rates are normalized by the flow required for minimum fluidization, which was experimentally determined to be 0.48 $\text{m}^3/\text{min} \pm 3\%$ for the 345 μm particles used in the present analysis. This measured value of the minimum fluidization velocity agrees to within 8% of the prediction from the correlation by Wen and Yu [25] for a bed without internals. This agreement suggests that the fluidization behavior of the present facility is typical of small particle fluidization in the absence of secondary flow.

4.1. Overall heat transfer coefficients

Fig. 5 shows normalized values of the overall heat transfer coefficient in the presence of a steady secondary flow; to acquire this data the primary flow was held constant while the secondary flow was varied. Overall heat transfer coefficients with a steady secondary flow, h_0, were normalized by the overall heat transfer coefficients measured with the primary flow only, h_p. The results are shown as a function of Q_t/Q_{mf}, the ratio of the total or combined flow rate of the primary and secondary streams over the flow rate required for minimum fluidization. Data acquired with the same primary flow rate are identified by like symbols and connected by

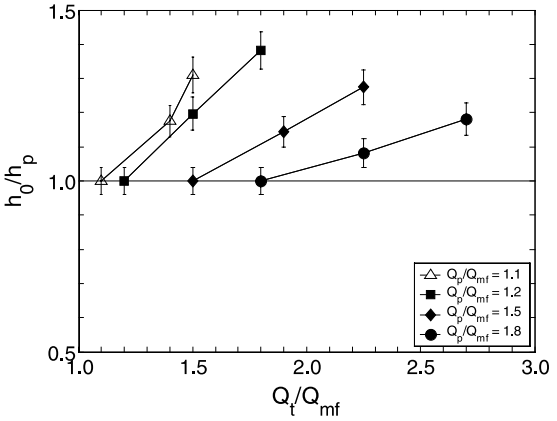

Fig. 5. Overall heat transfer for a combined primary and steady secondary flow condition compared with a primary flow condition.

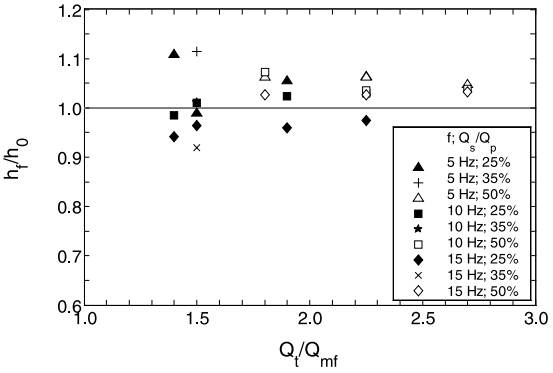

Fig. 6. Overall heat transfer for a combined primary and oscillating secondary flow condition compared with a combined primary and steady secondary flow condition (data include $Q_p/Q_{mf} = 1.1$, 1.2, 1.5, and 1.8).

solid lines. The figure shows that introduction of a steady secondary flow for a fixed primary flow rate resulted in increases in the heat transfer. In all cases, further enhancement of heat transfer resulted from increases in the secondary flow. The measured heat transfer enhancements were due to an increase in total air flow and/or the change in the fluidization hydrodynamics created by the steady, opposing secondary flow. The degree to which each factor influenced the observed increase in heat transfer cannot be determined from Fig. 5, but will be determined from a different normalization of the data.

To isolate and examine the effects of flow distribution on the heat transfer rate, h_0 is normalized by h_{eq}, the overall heat transfer coefficient associated with an equivalent flow condition. These normalized values, listed in Table 2, show that the dramatic increases in overall heat transfer observed in Fig. 5 were dominated by increases in the total rate of flow through the bed, as opposed to the hydrodynamic condition introduced by the secondary flow. In other words, under these operating conditions, essentially identical heat transfer rates resulted regardless of how the flow was distributed between the primary and secondary streams. This result provides an important basis for comparison when oscillations are imposed in the secondary flow stream.

To investigate the influence of the oscillating component of the secondary flow, independent of steady secondary flow hydrodynamics, overall heat transfer was measured with a superimposed oscillatory flow component having a frequency f. The resulting heat transfer coefficient is denoted as h_f and is normalized by h_0. This ratio is plotted in Fig. 6 as a function of Q_t/Q_{mf}. It should be noted that increases in the forcing frequency resulted in simultaneous increases in the velocity amplitude exiting the pulsed flow simulator tailpipe, as illustrated in Table 1. Hence, although reported as a function of forcing frequency, the results include the combined effects of velocity amplitude and forcing frequency. The results in Fig. 6 clearly show greater influences of the oscillating component at lower total flow rates. Although not conclusive, these results suggest that the combined energy of the oscillating and steady components of the secondary flow compared with the energy in the primary flow is an important factor in heat transfer enhancement. For example, at a Q_t/Q_{mf} of 1.5, the 5 Hz data show a dramatic change in h_f/h_0 with an increase in the secondary flow from 25% to 35% of the primary flow rate. However, the same increase in secondary flow rate for 10 and 15 Hz show a negligible change and a reduction in h_f/h_0, respectively, at the same total flow ratio. It is reasonable to expect the nonlinearities in the response of the bed to the ratio of energy between the primary and secondary flow contributed to this observed sensitivity to operating conditions.

Fig. 7 shows a nondimensional representation of the effects of the oscillating secondary flow on the

Table 2
Heat transfer for a steady secondary flow condition compared with the heat transfer for an equivalent flow condition

Q_p/Q_{mf}	Q_s/Q_p	$Q_t/Q_{mf} = Q_{eq}/Q_{mf}$	h_0	h_{eq}	h_0/h_{eq}
1.1	0.35	1.5	300	291	1.03
1.2	0.25	1.5	285	291	0.98
1.2	0.50	1.8	329	319	1.03

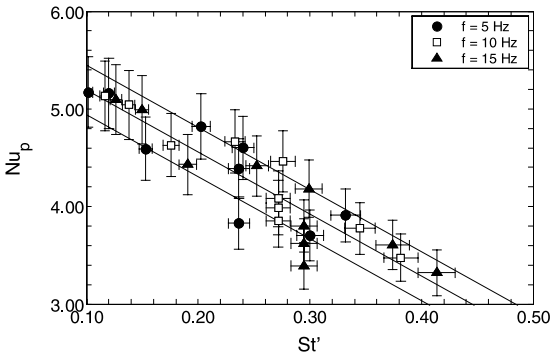

Fig. 7. Nondimensional heat transfer variations with forcing parameters.

particle Nusselt number. The nondimensional, independent variable is a modified form of the Strouhal number, which describes the increase in velocity amplitude associated with resonance in the pulsed flow simulator. The modified Strouhal number is defined as

$$St' = St\left(\frac{f}{f_n}\right)^{-0.8}, \tag{4}$$

where St is the Strouhal number

$$St = \frac{d_t f}{U_s} \tag{5}$$

and f and f_n are the forcing frequency and natural frequency of the pulsed flow simulator, respectively. Uncertainties in the Strouhal and Nusselt numbers were estimated to be 4% and 7%, respectively. Over the range of operating conditions represented in Fig. 7, the modified Strouhal number appears to correlate the fundamental behavior of the heat transfer. A least-squares linear curve was generated and is shown in Fig. 7 along with the standard limits of error for the curve fit (±0.24). The curve fit, exclusive of the steady secondary flow data, yields the equation $Nu_p = -6.35St' + 5.83$.

The general trend of Fig. 7 suggests that, for a fixed primary flow rate and fixed forcing frequency, an increase in the secondary flow rate yields an increase in the overall heat transfer coefficient. Also noted in Fig. 7 is that an increase in forcing frequency results in a decrease in the overall heat transfer coefficient, for fixed primary and secondary flow rates. These trends are also observed for most data in Fig. 6, with the greatest enhancement generally observed for a forcing frequency of 5 Hz. Of the forcing frequencies employed in the present study, 5 Hz was closest to the natural frequency of the bed which was determined experimentally by Pence et al. [2] to be 1.8 Hz. In the present facility, however, tests at pulse frequencies of 1.8 Hz were not possible due to controller and motor constraints.

4.2. Local, time-averaged heat transfer

A comparative analysis similar to that used to investigate the operating effects on the overall heat transfer coefficients is employed for the local, time-averaged heat transfer coefficients. Data reported in Figs. 8–12 are shown as a function of angular position. The angular position corresponding to 0° represents the stagnation point of the primary flow on the cylinder. As for the relation between the pulsed flow simulator and the hor-

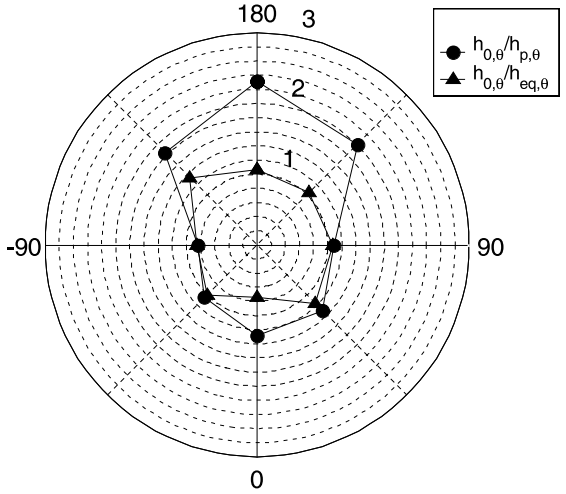

Fig. 8. Local heat transfer for a combined primary and steady secondary flow condition compared with a primary and equivalent flow condition ($Q_p/Q_{mf} = 1.1$, $Q_s/Q_p = 0.35$, $Q_t/Q_{mf} = Q_{eq}/Q_{mf} = 1.5$), (radical increments of 0.2).

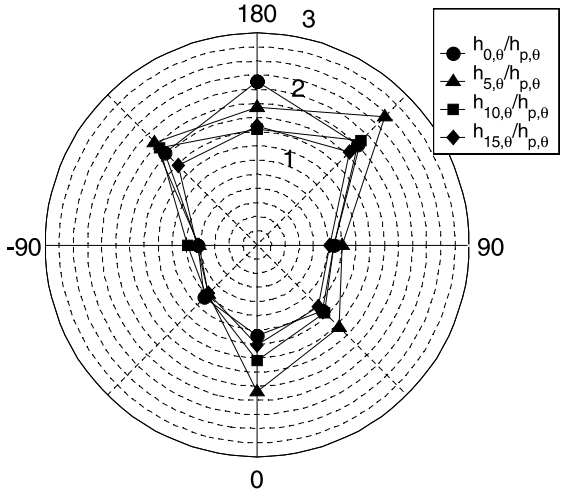

Fig. 9. Local heat transfer for a combined primary and oscillating secondary flow condition compared with a primary flow condition ($Q_p/Q_{mf} = 1.1$, $Q_s/Q_p = 0.35$, $Q_t/Q_{mf} = Q_{eq}/Q_{mf} = 1.5$), (radical increments of 0.2).

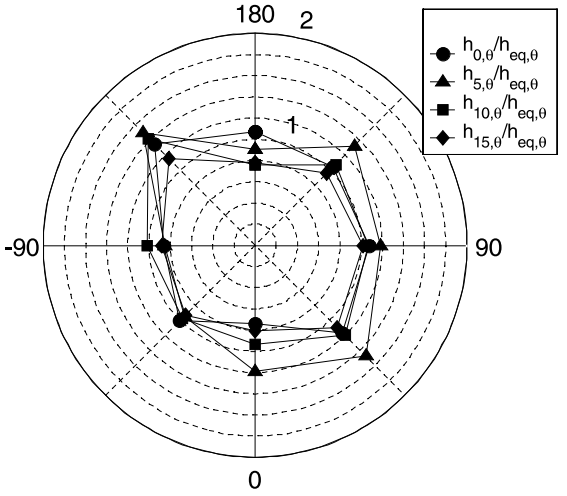

Fig. 10. Local heat transfer for a combined primary and oscillating secondary flow condition compared with an equivalent flow condition ($Q_p/Q_{mf} = 1.1$, $Q_s/Q_p = 0.35$, $Q_t/Q_{mf} = Q_{eq}/Q_{mf} = 1.5$), (radical increments of 0.2).

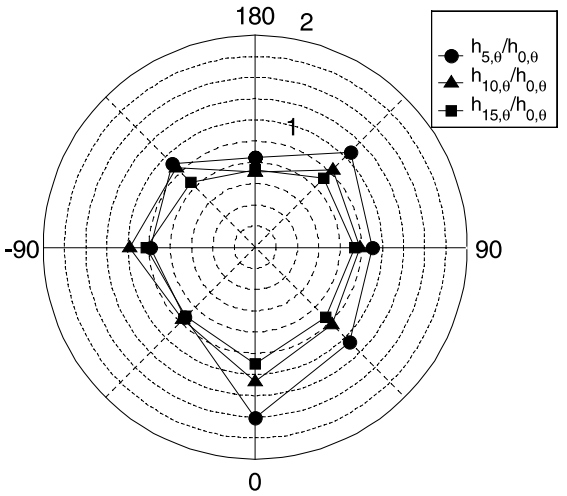

Fig. 11. Local heat transfer for a combined primary and oscillating secondary flow condition compared with a combined primary and steady secondary flow condition ($Q_p/Q_{mf} = 1.1$, $Q_s/Q_p = 0.35$, $Q_t/Q_{mf} = Q_{eq}/Q_{mf} = 1.5$), (radical increments of 0.2).

izontal cylinder, the center-to-center distance was 9.5 cm with the tailpipe located on the side of the cylinder corresponding to positive angular positions.

In Fig. 8, variations of $h_{0,\theta}/h_{p,\theta}$ as a function of θ are presented for data in which $Q_t/Q_{mf} = Q_{eq}/Q_{mf} = 1.5$, $Q_p = 1.1Q_{mf}$, and $Q_s = 0.35Q_p$. Enhancements in $h_{0,\theta}$ relative to $h_{p,\theta}$, a consequence of the secondary flow hydrodynamics and/or an increase in the total rate of

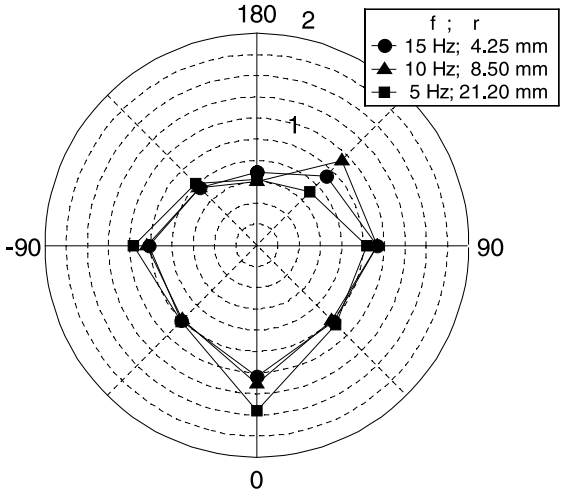

Fig. 12. Local heat transfer variations with forcing frequency $[h_{f,\theta}/h_{0,\theta}]$ ($Q_p/Q_{mf} = 1.1$, $Q_s/Q_p = 0.35$, $Q_t/Q_{mf} = Q_{eq}/Q_{mf} = 1.5$), (radical increments of 0.2).

flow, range from 30% at the stagnation point to 130% at the top of the cylinder, with significant enhancements also identified at ±135°. Also shown in Fig. 8 are values of $h_{0,\theta}$ normalized by $h_{eq,\theta}$. Such a normalization process isolates the secondary flow hydrodynamics. In the figure, local enhancements as great as 35% and diminishments near 20% in $h_{0,\theta}$ relative to $h_{eq,\theta}$ are observed with the redistribution of a fixed flow rate from one stream into two opposing streams. In contrast to overall heat transfer coefficients, which were unaffected by the secondary flow hydrodynamics, local time-averaged heat transfer coefficients were influenced by both increases in flow rate and the presence of a secondary stream.

Adding the influence of pulsing to the secondary flow, local time-averaged heat transfer coefficients measured with an oscillating secondary flow, $h_{f,\theta}$, and normalized by $h_{p,\theta}$ are plotted as a function of angular position in Fig. 9 for the flow conditions in which $Q_p/Q_{mf} = 1.1$, $Q_s/Q_p = 0.35$, and $Q_t/Q_{mf} = 1.5$. With the exception of the −45° and ±90° positions, significant enhancements in $h_{f,\theta}$ relative to $h_{p,\theta}$ resulted for forcing frequencies of 5, 10, and 15 Hz. Similar enhancements occurred for other operating conditions investigated using these particles. However, the superimposed forcing frequency had the most significant effect on local time-averaged heat transfer at the lowest primary fluidization ratio, Q_p/Q_{mf}, of 1.1.

Variations in $h_{f,\theta}/h_{eq,\theta}$ as a function of angular position are presented in Fig. 10. The operating conditions associated with Fig. 10 are identical to those in Fig. 9; however, the effects of increased flow rate previously included in Fig. 9 have been eliminated by the normalization used in Fig. 10. Enhancements in local heat

transfer coefficients, ranging from 20% to 50%, are observed at angular positions of 0°, +45°, +90° and ±135° for a forcing frequency of 5 Hz. As the forcing frequency was increased beyond 5 Hz, enhancements in heat transfer decreased at these angular positions while diminishments in heat transfer became more significant at other locations. Similar, yet substantially less pronounced trends for $h_{f,\theta}/h_{eq,\theta}$ as a function of θ and f resulted when Q_s/Q_p was decreased to a value of 0.25 for Q_t/Q_{mf} fixed at 1.5. Also, a reduction in Q_s/Q_p to 0.25 for Q_p/Q_{mf} held constant at 1.1 also yielded similar, but slightly less pronounced trends for $h_{f,\theta}/h_{eq,\theta}$ compared with those observed in Fig. 10.

To eliminate the effects of the hydrodynamic conditions introduced by a steady secondary flow and isolate the effects of the pulsation in the secondary flow, $h_{f,\theta}$ was normalized by $h_{0,\theta}$. The results for the operating conditions $Q_p/Q_{mf} = 1.1$ and $Q_s/Q_p = 0.35$ are shown in Fig. 11 as a function of θ. Significant enhancements in $h_{5,\theta}$ relative to $h_{0,\theta}$ are evident at 0°, +45°, and +135°. An increase on the order of 60% is observed at the stagnation position, with approximate 30% increases noted at +45° and +135°. As the forcing frequency was increased, less significant enhancements and more significant diminishments in $h_{f,\theta}$ compared with $h_{0,\theta}$ resulted for most angular positions. For the present particle distribution, there appears to be a significant dependence of local heat transfer on the pulsing characteristics, which include the effects of frequency and velocity amplitude of the secondary stream. The greatest effects were observed at the stagnation point and the side of the cylinder closest to the pulsed flow simulator tailpipe for a forcing frequency of 5 Hz.

In Figs. 8–11, local heat transfer coefficients were measured with a fixed linkage radius of 14.15 mm and, as noted by Table 1, increases in forcing frequency were accompanied by increases in velocity amplitude. To isolate the effect of forcing frequency, local time-averaged heat transfer data acquired with the velocity amplitudes of the secondary stream approximately equal were compared. The data in Fig. 12 are for 345 μm particles fluidized at $Q_p/Q_{mf} = 1.1$ and $Q_s/Q_p = 0.35$. Variations in $h_{f,\theta}/h_{0,\theta}$ are shown as a function of angular position. Estimated resonant velocity amplitudes of 16.5, 14.9, and 14 m/s were achieved by driving the piston at frequencies of 5, 10, and 15 Hz using flywheel radii of 21.2, 8.5, and 4.25 mm, respectively.

It is evident from Fig. 12 that for these primary and secondary flow rates, the frequency at which the opposing secondary flow was forced had relatively insignificant consequences on the local time-averaged heat transfer coefficient at all but the 0° and +135° positions. An enhancement on the order of 60% in local heat transfer at the stagnation point resulted for a forcing frequency of 5 Hz. Substantial reductions in $h_{f,\theta}$ occurred at −135° and 180° with the introduction of a forcing frequency when compared with $h_{0,\theta}$. At ±45°, the presence of an oscillating secondary flow had a negligible effect on $h_{f,\theta}$ when compared with $h_{0,\theta}$.

5. Conclusions

Heat transfer enhancement resulting from the introduction of an oscillating, opposing secondary flow in a bubbling gas-fluidized bed was experimentally determined. Increases in the overall heat transfer coefficient from a horizontal cylinder to the bed on the order of 40% were observed for 345 μm particles with the addition of a steady secondary flow. In the absence of imposed oscillations on the secondary flow, an increase in total flow was found to be the primary contributor to the observed heat transfer trends.

For the operating conditions investigated in the present study, redistribution of a fixed rate of flow through the plenum into two opposing streams resulted in no observable effect on overall heat transfer. However, with the redistribution of a fixed rate of flow through the plenum into two opposing streams, time-averaged values of local instantaneous heat transfer did show evidence of significant localized variations, which were a result of the hydrodynamic conditions created by the opposing secondary flow.

Observed enhancements and diminishments in overall heat transfer with superposition of an oscillatory waveform on a steady secondary flow depended upon both primary and secondary flow rates. For low primary and secondary flow rates and a forcing frequency of 5 Hz resulted in enhancements as great as 12% in overall heat transfer and 60% in time-averaged local heat transfer at the stagnation point. Of the forcing frequencies investigated, 5 Hz was closest to the natural frequency of the fluidized bed, which was 1.8 Hz. Because this natural frequency describes the overall hydrodynamics and pressure fluctuations associated with bubble formation, greater effects may be expected for imposed frequencies near the natural frequency of bubble formation.

The Strouhal number, modified by a normalized form of the forcing frequency, allowed a nondimensional representation of the particle Nusselt number for the present particle distribution, and operating conditions.

Acknowledgements

Support for this research from Manufacturing Technology Conversion International (MTCI), ThermoChem and the Morgantown Energy Technology Center through the South Carolina Institute for Energy Studies is gratefully acknowledged. The PAFBC technology was developed by MTCI and licensed to Ther-

moChem, with support from the US Department of Energy. The contributions of Dr. Momtez Mansour to the conceptual development and implementation of the PAFBC made this research possible. Dr. John Riester contributed significantly to the design of the present experimental facility, and the assistance of M. Cory Postle in the laboratory was invaluable. Special thanks are also extended to Kent Enfield for his assistance with the figures.

References

[1] M.N. Mansour, K. Dural-Swamy, R.R. Chandran, S. Shekarchi, J.N. Duqum, D.W. Warren, A.W. Hall, Pulsed atmospheric fluidized bed combustion, in: Proceedings of the 11th International Conference on Fluidized Bed Combustion, ASME, Montreal, Quebec, Canada, 1991, pp. 1351–1356.

[2] D.V. Pence, D.E. Beasley, M.C. Postle, Instantaneous pressure in pulse-stabilized fluidization, in: Proceedings of the Fluid Engineering Division Summer Meeting, ASME, San Diego, CA, 1996, pp. 855–860.

[3] D.V. Pence, D.E. Beasley, Chaos suppression in gas–solid fluidization, Chaos 8 (2) (1998) 514–519.

[4] M.L.M. van der Stappen, J.C. Schouten, C.M. van den Bleek, Application of deterministic chaos theory in understanding the fluid dynamic behavior of gas–solids fluidization, AIChE Symp. Ser. 296 (91) (1993) 91–102.

[5] C.S. Daw, J.S. Halow, Characterization of voidage and pressure signals from fluidized beds using deterministic chaos theory, in: Proceedings of the International Conference on Fluidized Bed Combustion, ASME, Montreal, Quebec, Canada, 1991, pp. 777–786.

[6] D.V. Pence, D.E. Beasley, J.B. Riester, Deterministic chaotic behavior of heat transfer in gas-fluidized beds, J. Heat Transfer 117 (2) (1995) 465–472.

[7] V.G. Ainshtein, N.I. Gel'perin, Heat transfer between a fluidized bed and a surface, Int. Chem. Eng. 6 (1) (1966) 67–74.

[8] N.S. Grewal, S.C. Saxena, Heat transfer between a horizontal tube and a gas–solid fluidized bed, Int. J. Heat Mass Transfer 23 (1980) 1505–1519.

[9] M. Kobayashi, D. Ramaswami, W.T. Brazelton, Pulsed-bed approach to fluidization, Chem. Eng. Prog. Symp. Ser. 66 (105) (1970) 47–57.

[10] M. Kobayashi, D. Ramaswami, W.T. Brazelton, Heat transfer from an internal surface to a pulsed bed, Chem. Eng. Prog. Symp. Ser. 66 (105) (1970) 58–67.

[11] W. Nowak, M. Hasatani, M. Derczynski, Fluidization and heat transfer of fine particles in an acoustic field, AIChE Symp. Ser. 89 (296) (1993) 137–149.

[12] N.A. Moussa, A.A. Fowle, Exploratory study of pulsed atmospheric fluidized bed combustion, in: Proceedings of the International Conference on Fluidized Bed Combustion, Department of Energy, Houston, TX, 1985, pp. 1300–1310.

[13] J.G. Yates, S.S. Cobbinah, D.J. Cheesman, S.P. Jordan, Particle attrition in fluidized beds containing opposing jets, AIChE Symp. Ser. 87 (281) (1991) 13–19.

[14] Z. Shen, C.L. Briens, M. Kwauk, M.A. Bergougnow, Study of a downward gas jet in a two-dimensional fluidized bed, Can. J. Chem. Eng. 68 (1990) 534–540.

[15] J. Ding, D. Gidaspow, A semi-empirical model for fluidization of fine particles, Indian Chem. Eng. 36 (4) (1994) 139–150.

[16] J.S.M. Botterill, Y. Teoman, K.R. Yuregir, Factors affecting heat transfer between gas-fluidized beds and immersed surfaces, Powder Technol. 39 (1984) 177–189.

[17] A.H. George, J.R. Welty, Local heat transfer coefficients for a horizontal tube in a large-particle fluidized bed at elevated temperature, AIChE J. 30 (3) (1984) 482–485.

[18] R. Chandran, J.C. Chen, F.W. Staub, Local heat transfer coefficients around horizontal tubes in fluidized beds, J. Heat Transfer 102 (1980) 152–157.

[19] Y. Kurosaki, H. Ishiguro, K. Takahashi, Fluidization and heat-transfer characteristics around a horizontal heated circular cylinder immersed in a gas fluidized bed, Int. J. Heat Mass Transfer 31 (2) (1988) 349–358.

[20] Y. Kurosaki, I. Satoh, T. Ishize, Mechanisms of heat transfer enhancement of gas–solid fluidized bed: estimation of direct contact heat exchange from heat transfer surface to fluidized particles using an optical visualization technique, J. Heat Transfer 117 (1995) 104–112.

[21] M. Kumada, S. Kume, I. Mabuchi, Y. Watanabe, M. Hirata, Characteristics of dynamic behavior and local heat transfer around single row tubes immersed in floating particles, Exp. Thermal Fluid Sci. 3 (3) (1990) 272–279.

[22] D.E. Beasley, R.S. Figliola, A generalised analysis of a local heat flux probe, J. Phys. E 21 (1988) 316–322.

[23] R.S. Figliola, M. Swaminathan, D.E. Beasley, A study of the dynamic response of a local heat flux probe, Meas. Sci. Technol. 4 (1993) 1052–1057.

[24] C. Dinu, D.E. Beasley, R.S. Figliola, Frequency response characteristics of an active heat flux gage, J. Heat Transfer 120 (3) (1998) 577–581.

[25] C.Y. Wen, Y.H. Yu, A generalized method for predicting the minimum fluidization velocity, AIChE J. 12 (3) (1966) 610–612.